Single-cell RNA sequencing uncovers the excitatory/inhibitory synaptic unbalance in the retrosplenial cortex after peripheral nerve injury

*Jing-Hua Wang[1,2+], Cheng Wu[1,2,3+], Yan-Na Lian[1,2+], Li Liu[4], Wei Chen[5], Wenjuan Chen[5], Zhi Zhang[6], Min Zhuo[7], Xiang-Yao LI [1,2]**

[1] Department of Neurobiology and Department of Psychiatry, Sir Run Run Shaw Hospital, Zhejiang University School of Medicine, Hangzhou 310016, China.

[2] NHC and CAMS Key Laboratory of Medical Neurobiology, Ministry of Education Frontier Science Center for Brain Research and Brain-Machine Integration, School of Brain Science and Brain Medicine, Zhejiang University, Hangzhou 310058, China.

[3]Zhejiang University-University of Edinburgh Institute, Zhejiang University School of Medicine, Haining 314400, China.

[4]Core Facilities of the School of Medicine, Zhejiang University, Hangzhou, Zhejiang 310058, China

[5]Department of Psychiatry, Sir Run Run Shaw Hospital, Zhejiang University School of Medicine, Hangzhou 310016.

[6]Key Laboratory of Brain Functions and Diseases, School of Life Science, University of Science and Technology of China, Hefei, Anhui 230027, China

[7]Department of Physiology, Faculty of Medicine, University of Toronto, Toronto, ON M5S 1A8, Canada.

[+]Equal contributors

[*] Correspondence:

Address correspondence to:

Dr. Xiang-Yao Li

Department of Neurobiology and Sir Run Run Shaw Hospital,

Room B715, Research Building, Zhejiang University School of Medicine,

866 Yuhangtang Road

Hangzhou, Zhejiang 310058, China

Phone: 86-571-8898-1693

E-mail: Lixiangy@zju.edu.cn

Running head: RSC regulates pain sensation

Number of tables: 0

Number of figures: 9

Number of pages: [44]

Number of words: Abstract (175); Introduction (664); Discussion (764)

Keywords: Chemogenetic approach; Retrosplenial Cortex; peripheral pain hypersensitivity; E/I balance; scRNA-seq

Abstract

Nerve injury in the somatosensory pathway may induce maladaptive changes in the transcriptional or protein levels that contribute to the development and maintenance of neuropathic pain. The retrosplenial cortex (RSC) processes nociceptive information, and it presents structural and molecular changes after nerve injury, in contrast, the detailed transcriptional changes in the RSC were unknown. Here we first confirm the involvements of RSC in the regulation of pain sensation and observe that the same peripheral stimulation activated more splenial neurons after nerve injury; decreasing the activities of CamkIIα^{+} splenial cells relieves peripheral pain hypersensitivity. Using a single-cell RNA-sequencing (scRNA-seq) approach, we identify the cell-type-specific gene's expressional changes after nerve injury. By analyzing the expression of ligand-gated ion channels, we observe the decreased *Gabar1a* but increased *Gria1*in the *CamkIIα*$^{+}$ neurons; consistently, we confirm the unbalanced excitatory/inhibitory synaptic transmissions by using the electrophysiological recording approach. Our data, therefore, provide information of the cell type-dependent transcriptomic changes in the RSC after nerve injury, which would help to understand the mechanisms of mediating neuropathic pain.

INTRODUCTION

Neuropathic pain caused by injury on the somatosensory pathway affects ~8% of people globally; it profoundly impairs the patients' life [1]. Unfortunately, the clinical management of neuropathic pain is still complex [2]. The maladaptive plasticity happens along the somatosensory pathway after nerve injury, from the dorsal root ganglion to the somatosensory cortex, which leads to pain hypersensitivity [3]. Nevertheless, the mechanisms that mediate these changes are complex. Multiple dysregulated molecular processes, such as gene transcription, protein translation, and protein post-translation modification, occur after nerve injury. Gene transcription after nerve injury contributes to irregular synaptic plasticity, abnormal neuronal excitability, and altered interbrain region connections, leading to the irregular pain sensation [4–6]. Knowing the transcriptional changes induced by nerve injury provides a novel window to understand the molecular mechanism of neuropathic pain.

The peripheral nerve injury may induce broadly transcriptomic changes in different types of cells. In the central nervous system (CNS), the glial cells, such as the astrocytes, oligodendrocyte, and microglia, have unique roles to maintain the brain's functions. Moreover, plenty of studies have shown that astrocytes and microglia had pathological changes, contributing to the development and maintenance of chronic pain [7,8]. The recently developed single-cell RNA sequencing (scRNA-seq) approach is helpful in the investigation of the heterogeneity of cell types. Using this approach, Xu Zhang's group identified ten types and 14 subordinate subtypes of somatosensory neurons in DRG of mice [9]. The results revealed the distinctive and sustained heterogeneity of transcriptomic responses to injury at a single neuron level [10]. Except for DRG neurons, the scRNA-seq approach was also applied to the spinal cord in the mouse neuropathic pain model to disclose new regulators of pain hypersensitivity and provide new therapeutic targets for neuropathic pain [11]. By screening differentially expressed genes in DRG of mice with spared nerve injury (SNI), activating transcription

factor 3 (ATF3) notably increased after SNI stimulation, which indicated that ATF3 plays an essential role in the progress of neuropathic pain and can be a candidate genetic marker to prognosticate and treat neuropathic pain [5]. Proto-oncogene Jun, function as a transcription factor, was also identified to interact with other genes strongly; it may serve as the prognostic and predictive genes of neuropathic pain [12]. Therefore, scRNA-seq provides a reliable and steady method to uncover the cellular heterogeneity and the candidate genetic marker in the progression of neuropathic pain caused by peripheral injuries.

The retrosplenial cortex (RSC) processes noxious information [13,14]. It has been shown that the RSC connects hippocampal formation and thalamus reciprocally, regulates the place navigation [15–17] and responses to nociceptive stimulations at physiological conditions [18]. Also, ~23% of RSC neurons respond to the cutaneous nociceptive stimulations on the anesthetized rabbits [13], peripheral pain stimulation enhanced regional cerebral blood flow (rCBF) [19] and induced rigorous emotion-like behaviors, following with a higher amount of c-Fos positive neurons in RSC of rat [20]. Furthermore, the spinal nerve ligation decreased the metabolism in the RSC of mice [21]. These observations indicate the metabolic and connectomes' changes occur in the RSC after nerve injury. Based on the previous studies, we proposed that the peripheral nerve injury may induce broadly transcriptional changes in the RSC; this may contribute to peripheral pain hypersensitivity. Here, we investigated this point in the RSC of a mouse model of neuropathic pain by combining a single-cell RNA sequencing approach. We identified the differentially expressed genes in different cell types. Our data provided a whole landscape of the transcriptomic changes in the RSC induced by nerve injury, which would help understand the molecular and cellular mechanisms for neuropathic pain.

Materials and methods

Experimental animals

Adult male C57B L/6 mice (8 weeks, weight: 20–35 g) were used in this study, and animals were housed four or five per cage at constant room temperature (21 ± 1 °C) and relative humidity (60 ± 5%) under a regular light/dark schedule (light 7.00 a.m.–7.00 p.m.), food and water were availed ad libitum. Before behavioral tests, the mice adapt to the laboratory conditions for about one week and adapt to the testing situation for at least 15 min before experiments. The animal care and use committee of Zhejiang University approved all mouse protocols.

Stereotaxic Virus Injection

AAV9-CamKIIα-hM3Dq-mCherry, AAV9-CamKIIα-hM4Di-mCherry, and AAV9-CamKIIα-mCherry were obtained from Vigene Biosciences (Shandong). Stereotaxic injections of AAVs were performed and adapted [22]. Briefly, mice were anesthetized with isoflurane (induction 4%, maintenance 1%) and the scalp was shaved and then cleaned with iodine (Triadine) and alcohol. The head of the mouse was fixed into a stereotaxic adapter mounted on a stereotaxic frame (Kopf model 962) and lubricant (Artificial Tears) was applied to the eyes. An incision was made over the skull and the surface was exposed. Two small holes were drilled above the RSC (AP: -2.30mm, ML: ±0.25mm, VD: -1.20mm), and the dura was gently reflected. Virus was infused at a rate of 20 nl per min. Following infusion, the needle was kept at the injection site for 10 min and then slowly withdrawn. The total volume of virus infused was based on its titer.

Common Peroneal Nerve (CPN) Ligation Model

The CPN ligation was performed as described previously [23]. Briefly, mice were anesthetized with isoflurane (1-3%, as needed). The left CPN was slowly ligated between the

anterior and posterior groups of muscles with chromic gut suture 5-0 (Ethicon) until the appearance of twitching of the digits. The skin was sutured with 5-0 silk and cleaned with povidone iodine. Sham surgery was carried out in the same manner, but the nerve was not ligated. All animals were kept in their home cages after surgery.

Behavioral tests

Mechanical Allodynia Test

On an experimental day, the von Frey behavioral assay was performed according to the up-down algorithm described by Dixon [24]. To determine evoked reflex responses to mechanical stimuli, animals were placed on a raised mesh grid and covered with a clear plastic box for containment. Calibrated von Frey filaments were applied to the middle of the plantar surface of each paw until the filament bent. Brisk withdrawal or paw flinching was considered a positive response. Lifting of the paw due to normal locomotor behavior was ignored. In the absence of a response, the filament of the next greater force was applied. Following a response, the filament of the next lower force was applied. The tactile stimulus producing a 50% likelihood of withdrawal was calculated and treated as the paw withdraw threshold (PWT).

Conditioned Place Preference/aversion

We performed a conditioned place preference (CPP) test, as described previously [25]. Briefly, mice were pre-conditioned for three days: they were allowed to explore the chamber freely for 10 min on the first two days; a video camera recorded the behaviors on the third day, and we analyzed the time spent in each chamber; the following day, we injected the control solution paired with a randomly-chosen chamber in the morning, and the appropriate drug treatment paired with the other chamber 4 hrs. later (in the afternoon). Twenty hours after the afternoon pairing, we placed mice in the CPP box with access to all chambers and analyzed their behavior recorded for 15 min for chamber preference. We calculated the preference

index as the time spent in the drug-paired chamber minus the time spent in the vehicle-paired chamber.

Novel object recognition

Novel object recognition test was adapted from a behavioral paradigm reported by Leger M. et al. [26]. Described briefly, we put mice into the three chambers instruments for five minutes for the habituation first. Twenty-four hours later, we put two identical bottles into the center of the two chambers and allowed mice to explore them for five minutes. We replaced one of them by a new bottle with a different shape twenty-four hours later and allowed mice to explore freely for five minutes, and recorded the time spent to explore the old or new bottle, respectively. We calculated the discrimination index (DI) as the time difference between the new bottle and the old bottle.

Elevated plus maze test.

Elevated plus maze has been validated to assess the anti-anxiety effects and to define the brain regions and animals' behavior related to anxiety. Thirty minutes after the application of CNO, the mouse was placed on the junction of closed and open arms and its head faced the open arm. Then, start the video-tracking system and record for 5 min.

Open Field Test

White plastic boxes were used as open-field chambers (dimensions: 45 × 45 × 45 cm^3). Mice were individually placed in the center of a chamber and allowed to explore for 10 min freely. The locomotor and exploratory behaviors were recorded with ANY-maze software (Stoelting, Wood Dale, IL 60191, USA). The total distance traveled was used to evaluate locomotor activity.

Whole-cell Patch-clamp Recording

Coronal brain slices (300 μm) at the level of the RSC from mice with sham surgery or CPN ligation were prepared using standard methods. Slices were transferred to a submerged

recovery chamber with oxygenated (95% O_2 and 5% CO_2) artificial cerebrospinal fluid (ACSF) containing (in mM) 124 NaCl, 2.5 KCl, 2 $CaCl_2$, 1 $MgSO_4$, 25 $NaHCO_3$, 1 NaH_2PO_4, and 10 glucose at room temperature for at least 1 h. Experiments were performed in a recording chamber on the stage of a microscope equipped with infrared differential interference contrast optics for visualization. Evoked excitatory postsynaptic currents (EPSCs) were recorded from layer II/III neurons of the RSC with an Axon 700B amplifier, α-Amino-3-hydroxy-5-methyl-4-isoxazolepropionic acid receptor (AMPAR)-mediated spontaneous EPSCs were recorded in voltage-clamp model with membrane potentials holding at –60 mV in the presence of AP5 (50 μM). The recording micropipettes (3-5 MΩ) were filled with a solution containing (in mM) 124 K-gluconate, 5 NaCl, 1 $MgCl_2$, 0.2 EGTA, 10 HEPES, 2 MgATP, 0.1 Na_3GTP, and 10 phosphocreatine disodium (adjusted to pH 7.2 with KOH). Picrotoxin (100 μM) was used to block γ-aminobutyric acid A receptor-mediated inhibitory synaptic currents in all experiments. The initial access resistance (15–30 MΩ) was monitored throughout experiments. Data were discarded if the access resistance changed >15% during an experiment. Data were filtered at 1 kHz and digitized at 10 kHz.

Immunostaining

Mice were anesthetized with 1% pentobarbital sodium and perfused transcardially with 0.1 M phosphate-buffered saline (PBS) followed by 4% paraformaldehyde (PFA) in PBS. Brains were post-fixed overnight in PFA at 4°C. Each brain was then dissected and further fixed in 4% PFA for an additional 24 h, and then transferred to 15% sucrose in PB followed by 30% sucrose until saturated. The brain was embedded in Tissue-Tek OCT compound, frozen in liquid nitrogen, and stored at -80 °C before being cut into 25 μm coronal sections in a cryostat at –20°C (CM3050S, Leica). Free-floating sections were washed with PBS. For immunostaining, sections were incubated with blocking buffer (5% normal goat serum and 0.3% Triton X-100 in PBS) for 1 h at room temperature, and incubated with primary antibody

(c-Fos, 1:1000; #2250, Cell Signaling Technology, Danvers, US) overnight at 4°C. Sections were washed in PBS and then incubated with the appropriate secondary antibody (goat anti-rabbit 488; 1937195, Life Technologies) for 2□h at room temperature. Sections were washed again for 3×10 min in PBS. After washing, they were mounted on coverslips using Fluoroshield mounting medium with DAPI (ab104139, Abcam, Cambridge, UK) for image collection.

Cell isolation

We obtained single cells according to a previous protocol [27]. Individual adult male mice were anesthetized with isoflurane and decapitated. We removed the brain and rapidly dissected out the RSC. We put the RSCs from two mice together, then cut the tissue into small pieces and transferred them to a 1.5ml microcentrifuge tube with 3mg/ml isolation solution, containing pronase (Sigma, Cat#P6911-1G),1% BSA and 50μg/ml DNaseI (Sigma, cat. no. D5025) in 1ml HibernateA (Invitrogen, cat. no. A1247501)/B27 (Invitrogen, cat. no. 17504) medium (HABG). The tissue and solution were mixed for 30min at 37□ in the horizontal shaker with 200 g. After incubation, we gently triturated the fabric with polished tips, and the single cells were released. The purified cells were obtained by density gradient centrifugation at 800 g for 15 min and re-suspended in 1xPBS (calcium and magnesium-free) containing 1% BSA, then centrifuged at 200 g for 2 min. The single cells were concentrated and re-suspended in the desired medium. Cell number and healthy state were measured by trypan blue staining.

RNA library preparation for high-throughput sequencing

Thousands of cells were partitioned into nanolitre-scale Gel Bead-In-Emulsions (GEMs) using 10x GemCode Technology, where cDNA produced from the same cell shares a common 10x Barcode. Upon dissolution of the single-cell 3′ gel bead in a GEM, primers containing an Illumina R1 sequence (read1 sequencing primer), a 16-bp 10x Barcode, a 10-bp

randomer, and a poly-dT primer sequence were released and mixed with cell lysate and Master Mix. After incubation of the GEMs, barcoded, full-length cDNA from poly-adenylated mRNA was generated. Then the GEMs were broken, and we used silane magnetic beads to remove excess biochemical reagents and primers. Before library construction, we used enzymatic fragmentation and size selection to optimize the cDNA amplicon size. P5, P7, a sample index, and R2 (read two primer sequences) were added to each selected cDNA during end repair and adaptor ligation. P5 and P7 primers were used in Illumina bridge amplification of the cDNA (http://10xgenomics.com). Finally, the library was sequenced into 150-bp paired-end reads using the Illumina HiSeq4000.

Data processing of scRNA-seq

The analysis of single-cell RNA-seq was similar to the previous study [28], described briefly, cell ranger 2.0.1 (http://10xgenomics.com) was used to perform quality control and read counting of Ensemble genes with default parameters (v2.0.1) by mapping to the mm10 mouse genome. We excluded weak quality cells after the gene-cell data matrix was generated by Cell Ranger software using the Seurat package (v3.1.2). Only cells that expressed more than 200 genes and fewer than 7,000 genes were considered, and only genes expressed in at least three single cells (0.1% of the raw data) were included for further analysis. Exclude cells that expressed hemoglobin genes (*Hbm*, *Hba1*, *Hba2*, *Hbb*, *Hbd*, *Hbe1*, *Hbg1*, *Hbg2*, *Hbq1*, and *Hbz*). Discard cells with a mitochondrial gene percentage over 10%. In total, 20,169 genes across 23,315 single cells remained for subsequent analysis. Normalize data to a total of $l \times 10^4$ molecules per cell for the sequencing depth using the Seurat package. The batch effect was mitigated by using the ScaleData function of Seurat (v3.1.2).

Identification of cell types and subtypes by dimensional reduction

On day 7 after CPN ligation or sham treatment, we conducted cell isolation and performed single-cell RNA sequencing experiments. Use the Seurat package (v3.1.2) to

perform the linear dimensional reduction [28]. We just included the clusters with cells and finally got 31,146 single cells for further analysis (Ctrl: 7,965 and 11,296 cells; CPN: 5,966; and 5,919 cells) by 10X-genomics single-cell RNA sequencing (scRNA-seq). We selected 2000 highly variable genes as input for PCA. Then we identified significant PCs based on the JackStrawPlot function. Strong PC1–PC20 was used for t-SNE to cluster the cells by FindClusters function with resolution 0.5. We further constructed the K-Nearest Neighbor (KNN) graph based on Euclidean distance in PCA space and clustered cells by the Louvain algorithm. We excluded the clusters with less than 100 cells and that have cells from one group. Clusters were identified by the expression of known cell-type markers. We combined the SingleR results and the expression of the following markers to annotate the cell types: *Pdgfra, Cldn5, Cx3cr1, Gja1, Cldn11, Acta2, Pf4, and Kcnj8* to classify oligodendrocyte precursor cells (OPCs), endothelial cell, microglia, astrocyte, oligodendrocyte, vascular smooth muscle cell (vSMC), macrophage and pericyte, respectively. The clusters that mainly expressed the *CamkIIα* and *Thy1* were treated as neurons.

Identification of DEGs

The DEGs of each cluster were identified using the FindMarkers function (thresh.use = 0.25, test.use = “bimod”) with the Seurat R package [29]. We used the Wilcoxon rank-sum test (default) and selected genes with average expression difference > 0.25 natural log with $P < 0.05$ as marker genes. The DEGs of each part of cells were identified using the FindMarkers function (thresh.use = 0.18, test.use = “ wilcox ”) with the Seurat R package. [29] We used the Wilcoxon rank-sum test (default) and selected genes with average expression difference > 0.25 log fold-change of the average expression with $P < 0.05$ as DEGs. The GO analysis and GSEA was performed with the Clusterprofiler R package (V3.16.1) [30]. The cell-cell communications were performed using the iTALK [31].

Data availability

The scRNA-seq data used in this study would be deposited as the requirements of editorial policy. Raw image files used in the figures that support the findings of this study are available from the corresponding authors upon reasonable request.

Data Analysis

Off-line analysis on whole-cell patch-clamp data was performed using Clampfit 10. GraphPad Prism 8.0 was used to plot and fit the data. Statistical comparisons were made using Student's *t*-test, one - way ANOVA or two - way ANOVA (Tukey's test, Bonferroni's test, or Sidak's test was used for *post hoc* comparison) or the Kruskal - Wallis test (Dunn's Multiple Comparison Test was used for *post hoc* comparison). All data are presented as the mean ± SEM. In all cases, $P < 0.05$ was considered statistically significant.

RESULTS

Enhancing the Activities of CamKIIα$^+$ neurons in RSC via chemogenetic approach induced place aversion in naïve mice

Here we evaluated the role of RSC in the regulation of pain sensation by manipulating the activities of the alpha subunit of calcium / calmodulin-dependent protein kinase type II (CamKIIα$^+$) neurons. We expressed the human M3 muscarinic DREADD receptor coupled to Gq (hM3Dq) on the CamKIIα$^+$ neurons (CamKIIα-hM3Dq-mCherry) in RSC via adeno-associated virus (AAV) and AAV9-CamKIIα- mCherry as a control **(Figure 1A)**, binding of Clozapine-N-oxide (CNO) to this receptor increases neuronal excitability. Three weeks after the virus injection, we examined CNO's effects by using the whole-cell patch-clamp recording approach. As shown in **Figure 1B and C**, CNO significantly increased the number of action potentials (APs) in hM3Dq expressed neurons (**Figure 1C**). Behaviorally, the systemically application of CNO decreased the paw withdraw thresholds (PWTs), and this effect lasted for less than two hours (**Figure 1D and E**). Furthermore, the CNO also shortened thermal withdrawal latency (**Figure 1F**). Therefore, activating the CamKIIα$^+$ neurons in RSC of mice sensitized both mechanical and thermal sensation.

Given that RSC's neuronal activities are necessary for the aversive memory [32], whether activating the CamKIIα$^+$ neurons would also cause aversion? We examined this point by using a conditioned place behavioral approach (**Figure 1G**). In the pre-conditioning session, the mice with or without hM3Dq expression spent equal time exploring the chambers **(Figure 1H**). While in the test session, unlike the mice with the control virus, the mice with hM3Dq spent less time in the CNO paired chamber (**Figure 1H**). These data suggest that activating the CamKIIα$^+$ neurons in RSC is sufficient to induce aversion. Furthermore, the CNO application did not change the time spent in the center zone (**Figure 1I and J**) and traveling distance (**Figure 1K**) in the open field test, indicating that activating RSC CamKIIα$^+$ neurons

did not affect anxiety. Furthermore, we examined the expression of c-Fos, an immediate-early gene, and observed that the CNO application increased the number of c-Fos positive cells in the RSC of mice with hM3Dq expression (**Figure 1L and M**). In summary, activating the CamKIIα^{+} neurons in RSC via the chemogenetic approach sensitized the mechanical sensation and induced aversion in naïve mice.

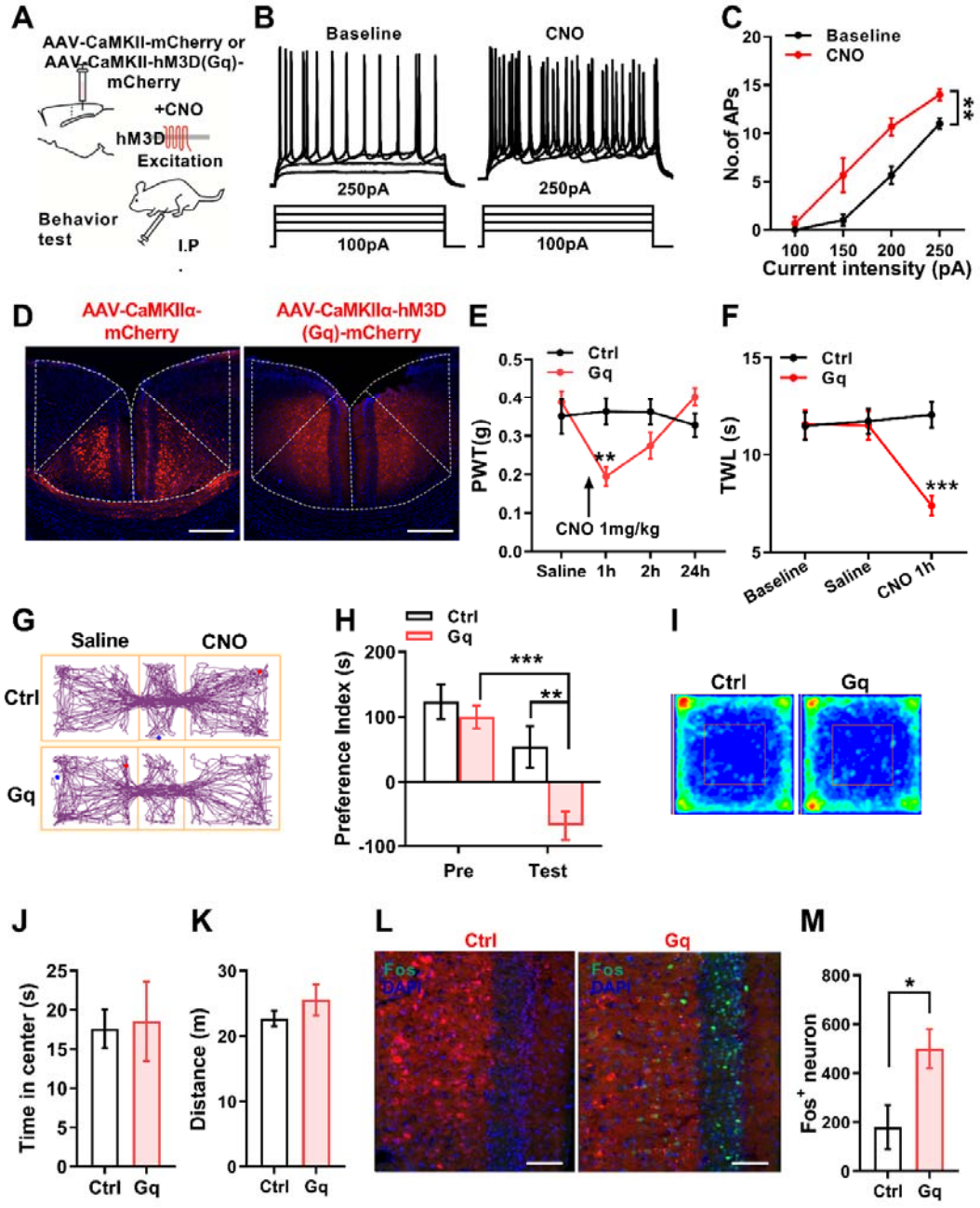

Figure 1. Activating the CamKIIα^{+} neurons in RSC decreased PWTs and induced conditioned place aversion

(A) A diagram to show the experiment design of the hM3Dq expression.

(B) Represented traces showed that CNO's application increased the number of action potentials in the hM3Dq expression neurons. Raw traces show individual voltage responses to 500ms current pulse from 100pA to 250pA with 50pA steps.

(C) Summarized data showed that the application of CNO increased the excitability of hM3Dq expression neurons. (3 neurons from 2 mice, two-way ANOVA, $F_{(1,4)} = 9.38$, $P < 0.05$)

(D) Representative images showed the expression of control or hM3Dq -mcherry in the RSC.

(E) The application of CNO decreased the paw withdrew thresholds (PWT) of mice with hM3Dq expression and recovered after 24 hours. (Two-way ANOVA, Interaction, $F_{(3, 92)} = 6.39$, $P < 0.01$; time, $F_{(3, 92)} = 3.69$, $P < 0.05$; Ctrl *vs*. hM3Dq, $F_{(1, 23)} = 2.19$, $P > 0.05$; Sidak's multiple comparisons test, Ctrl *vs*. hM3Dq (1h): $P < 0.01$; Ctrl *vs*. hM3Dq (2h): $P > 0.05$, n = 10 for Ctrl, n =15 for HM3Dq).

(F) The application of CNO extended the paw withdrew latency (PWL) of mice with hM3Dq expression. (Two-way ANOVA, Interaction, $F_{(2, 54)} = 8.26$, $P < 0.01$; time, $F_{(2, 54)} = 6.33$, $P < 0.01$; Ctrl *vs*. HM3Dq, $F_{(1, 27)} = 5.63$, $P < 0.05$; Sidak's multiple comparisons test, Ctrl *vs*. HM3Dq (1h): $P < 0.01$; n = 16for Ctrl, n =13 for HM3Dq).

(G) Representative traveling traces of the Ctrl and hM3Dq group mice in the conditioned place aversion test.

(H) The application of CNO to the hM3Dq group induced place aversion. (Two-way ANOVA, Interaction, $F_{(1,19)} = 5.278$, $P < 0.05$; time, $F_{(1,19)} = 30.41$, $P < 0.001$; Ctrl vs. hM3Dq , $F_{(1,19)} = 6.822$, $P < 0.05$, Ctrl, n = 10, hM3Dq , n = 11. Sidak's multiple comparisons test, Ctrl *vs*. hM3Dq (Test): $P < 0.01$; Pre *vs*. Test (hM3Dq): $P < 0.001$).

(I) Heat map diagram showing the traveling traces of both groups in the open field test.

(J) The application of CNO did not change the time in the center area in the open field test. (Unpaired *t*-test, $P > 0.05$).

(K) In the open field test, hM3Dq group mice traveled a similar distance compared to Ctrl after applying CNO. (Unpaired *t*-test, $P > 0.05$).

(L) Representative images of the c-Fos expression induced by CNO injection in the RSC of naïve mice. (Scale bar, 200 μm).

(M) The application of CNO increased c-Fos expression in the hM3Dq group. (Unpaired *t*-test, $P < 0.05$).

CPN ligation altered the neuronal activities in RSC that contribute to the pain hypersensitivity.

Peripheral nerve injury caused structural and metabolic changes in the RSC [33], indicating the abnormal neuronal activities after pain stimulation. To confirm this assumption, by employing a mouse model of neuropathic pain with ligation on the common peroneal nerve (CPN) [32], we examined the expression of c-Fos in RSC after mechanical stimulation with von Frey filament (0.4 g). As shown in **Figure 2A** and **B**, we observed a higher amount of c-Fos positive neurons after the mechanical stimulations at day seven after CPN ligation. The anterior cingulate cortex (ACC) is vital to pain regulation [34]; we also checked the expression of c-Fos in the ACC as a positive control and observed a similar change, but not in the hippocampus (**Figure 2A and B**). Furthermore, about 92% of c-Fos positive neurons expressed the CamKIIα (**Figure 2C and D**). The mechanical stimulation with the same strength activated more CamKIIα$^+$ neurons in the RSC of mice with CPN ligation than in the control group.

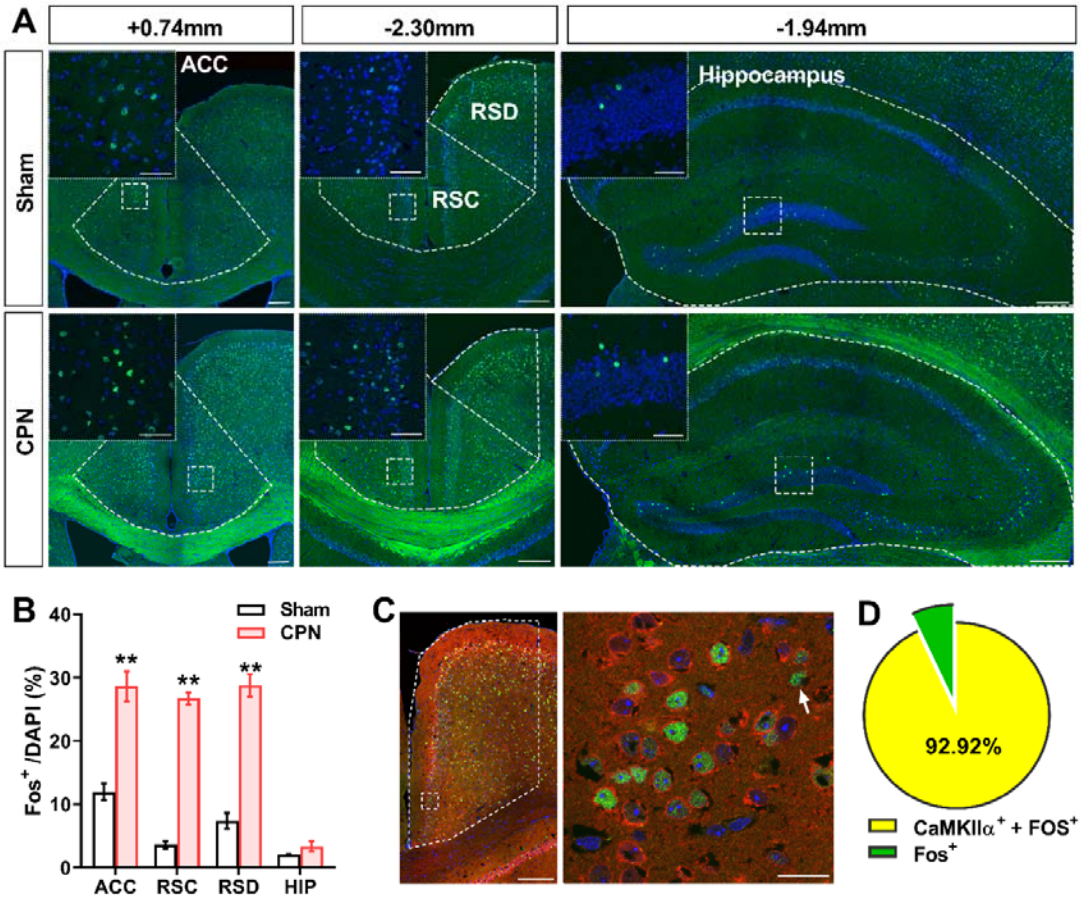

Figure 2. Mechanical stimulation activated more neurons in the RSCs of mice with CPN ligation.

(A) Examples showing the expression of c-Fos in different brain regions of the Sham or CPN group. Inset, region magnification. (Bottom Scale bar, 200 μm; top left: 50 μm).

(B) Quantification of c-Fos positive cells within the ACC, RSC, and hippocampus (Hip), there were more c-Fos positive cells in the ACC and RSC, but not in the hippocampus in mice with CPN ligation. (Two-way ANOVA, interaction, $F_{(3,31)} = 32.19$, $P < 0.01$; regions, $F_{(3,31)} = 79.95$, $P < 0.01$; sham *vs*. CPN, $F_{(1,31)} = 311.90$, $P < 0.01$, Sham, n = 5, CPN, n = 5.), ** indicates $P < 0.01$

(C) C-Fos and CamKIIα co-immunostaining results in RSC. (Left panel, scale bar, 200 μm; right panel, scale bar, 20 μm).

(D) About 93.0% of c-Fos positive cells were CamKIIα^{+} cells.

Do the RSC's enhanced neuronal activities contribute to the pain hypersensitivity after nerve injury? We selectively inactivated the CamKIIα-positive neurons and examined mechanical allodynia effects in mice. We expressed the human M4 muscarinic DREADD receptor coupled to Gi (hM4Di) in RSC (**Figure 3A**). Unlike the hM3Dq, the CNO binding to hM4Di inhibits neuronal activities. We delivered the AAV9-CamKIIα-hM4Di-mCherry into RSC. The CNO application did decrease the number of firing APs examined via the whole-cell patch-clamp recording approach (**Figure 3B and C**). In the animals with the control or hM4Di expression, we performed CPN ligation, which decreased the PWTs of both groups (**Figure 3D and E**). The CNO application increased the PWTs of mice with hM4Di expression but not that with the control virus (**Figure 3E**). Similarly, the CNO also extended the thermal withdrawal latency in the hM4Di expression mice with CPN ligation (**Figure 3F**). These observations indicate that the enhanced neuronal activities in the RSC contribute to the peripheral mechanical and thermal sensitivities after nerve injury.

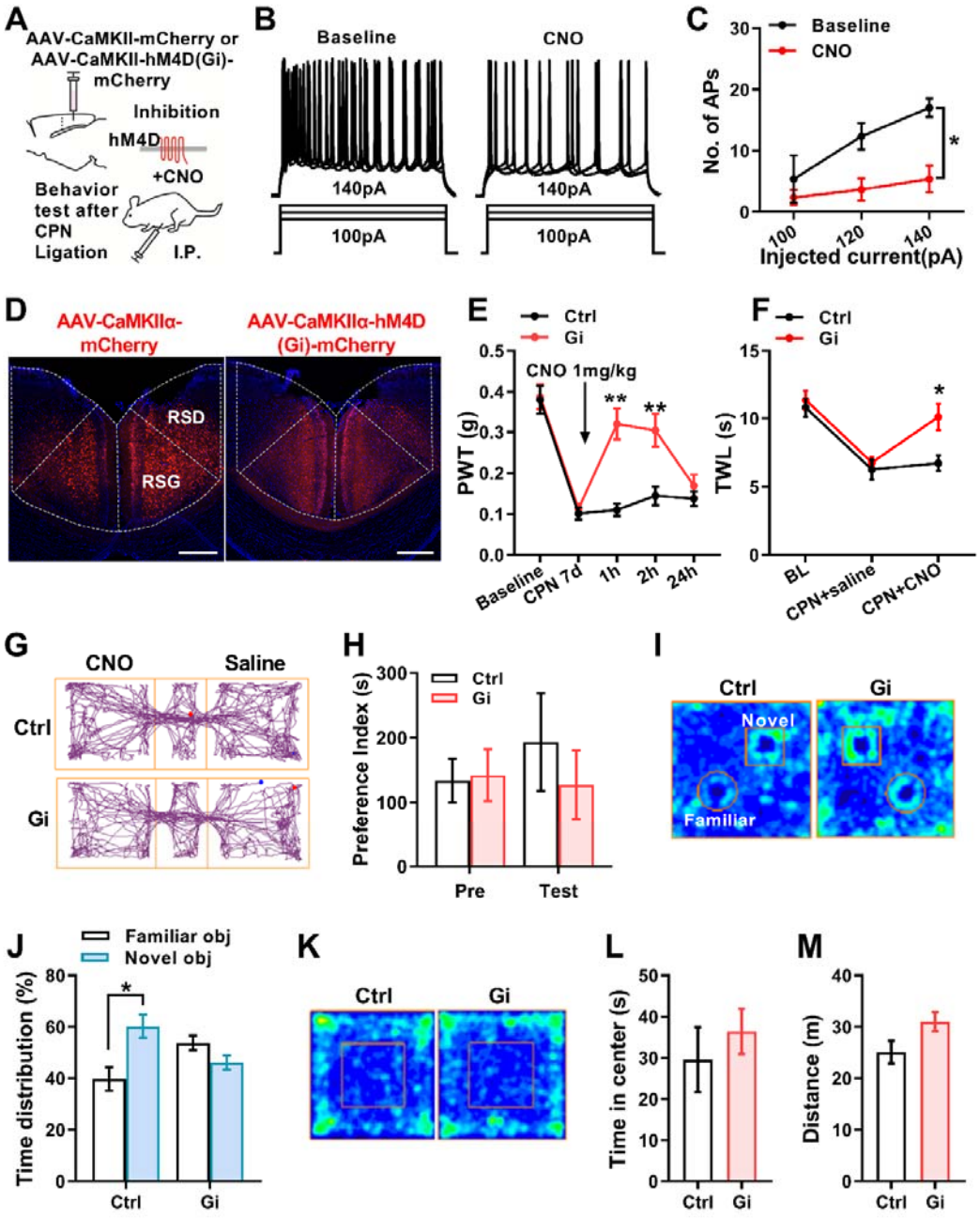

Figure 3. Inactivating CamKIIα^{+} neurons in RSC increased PWTs and TWL.

(A) The diagram showed the experiment design of hM4Di expression.

(B) Represented traces showed that the application of CNO decreased the number of action potentials in the hM4Di-expressing neurons. Raw traces show individual voltage responses to 500 ms current pulse from 100 pA to 140 pA with 20 pA steps.

(C) Summarized data showed that the application of CNO increased the excitability of hM4Di expression neurons. (two-way ANOVA, interaction, $F_{(2,8)}$ = 2.92, P >0.05; currents, $F_{(1.1,4.4)}$ = 8.16, P <0.05; baseline *vs.* CNO, $F_{(1,4)}$ = 9.92, P <0.05, 3 neurons from 2 mice)

(D) Representative images showed the expression of control or hM4Di-mcherry in the RSC. (Scale bar, 200 μm).

(E) CPN ligation decreased PWTs of both Ctrl and hM4Di groups, and the application of CNO (i.p.) increased the PWTs of hM4Di group significantly, then completely recovered after 24 hours, it has no effects on the Ctrl group. (Two-way ANOVA, interaction, $F_{(4,116)}$ = 6.72, P <0.01; time, $F_{(4,116)}$ = 33.51, P <0.001; Ctrl *vs*. HM4Di, $F_{(1,29)}$ = 15.29, P <0.01, n = 15 for Ctrl and n = 16 for HM4Di. Sidak's multiple comparisons test, Ctrl *vs*. HM4Di (1h): **P < 0.01).

(F) CPN ligation decreased PWL of both groups, and the application of CNO (i.p.) increased the PWL of HM4Di group significantly. (Two-way ANOVA, interaction, $F_{(2,30)}$ = 3.15, P >0.05; time, $F_{(1.96,29.37)}$ = 24.44, P <0.001; Ctrl *vs*. HM4Di, $F_{(1,15)}$ = 5.50, P <0.05, n = 9 for Ctrl and n = 8 for HM4Di. Sidak's multiple comparisons test, Ctrl *vs*. HM4Di (1h): *P < 0.05).

(G) Representative traveling traces of Ctrl and HM4Di group mice in the conditioned place preference test.

(H) The application of CNO did not induce place preference on HM4Di group of mice in the CPP test. (Two-way ANOVA, Interaction, $F_{(1,9)}$ = 0.91, P > 0.05; time, $F_{(1,9)}$ = 0.33, P > 0.05; Ctrl *vs*. HM4Di, $F_{(1,9)}$ = 0.21, P > 0.05, Ctrl, n = 5, HM4Di, n = 6).

(I) Heat map diagram showing the traveling traces in the novel object recognition test.

(J) One hour after I.P. of CNO, Ctrl, and HM4Di group mice explored two identical objects for 5 minutes, 24 hours later, HM4Di group mice spent similar time exploring familiar and novel objects while Ctrl group mice explored novel object longer. (Two-way ANOVA, Interaction, $F_{(1,10)} = 6.83$, $P < 0.05$; Ctrl *vs.* HM4Di, $F_{(1,10)} = 169.00$, $P < 0.001$; Familiar *vs.* Novel, $F_{(1,10)} = 1.45$, $P > 0.05$, n = 6 for both groups; Sidak's multiple comparisons test, Familiar *vs.* Novel (Ctrl): $P < 0.05$).

(K) Heat map diagram showing the traveling traces of both groups in the open field test.

(L) In the open field test, HM4Di group mice moved a similar distance compared to Ctrl 1 hour after applying CNO. (Unpaired *t*-test, $P > 0.05$).

(M) In the open field test, HM4Di and Ctrl group mice spent similar time in the center zone one hour after applying CNO. (Unpaired *t*-test, $P > 0.05$).

The single-cell landscape of RSC cells

In examining the cell type-dependent transcriptomic changes induced by CPN ligation in the RSC, we first isolated the RSC cells and analyzed the transcriptomic characteristic of splenial cells using a single-cell RNA-sequencing (scRNA-seq) approach (**Figure 4A**). Then, we compared the genes expressional difference between mice with or without CPN. Since we planned to analyze the difference between two groups, we just included the clusters with cells and finally got 31,146 single cells for further analysis (Ctrl: 7,965 and 11,296 cells; CPN: 5,966; and 5,919 cells) that belong to eight types of cells (**Figure 4B, Figure S1a**) based on the expression of classic cell types markers (**Figure 4C**), including the endothelial cells (ECs), microglia (Micro), oligodendrocytes precursor cells (OPC), oligodendrocytes (Oligo), astrocytes (Astro), *CamkIIα*$^{+}$ neurons that highly expressed *CamkIIα*, vascular smooth muscle cells (vSMC) and macrophages (Mac). Then, using the FindAllMarkers function of Seurat, we identified the featured differential expression genes (fDEGs) of each cell type (**Figure 4D**,

Stable 1, **Figure S1b**). The gene ontology (GO) analysis showed that the top100 fDEGs are different on the biological processes (BP) (**Figure 4E** & **Stable 2**) and molecular functions (MF) (**Figure 4F** & **Stable 3**).

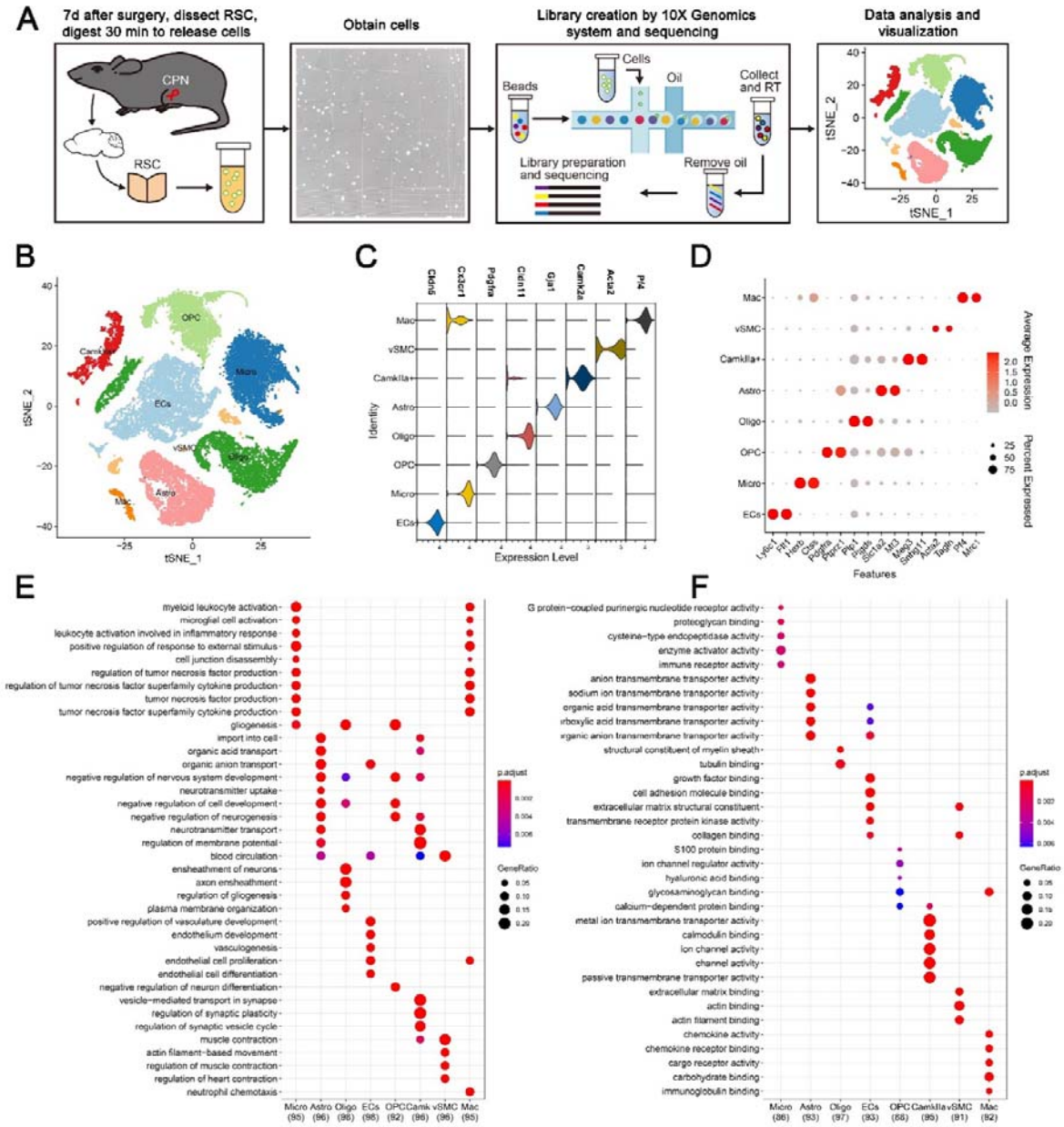

Figure 4. The transcriptomic profiles of single cells in the RSC with or without CPN ligation.

(A) Overview of the experimental workflow for the single-cell RNA sequencing.

(B) *t*-SNE embedding projection of nine types of cells from the RSC of adult mice.

(C) Vlnplot to show the cell-type dependent expression of cell types markers.

(D) Dot plot showing the expression of top 2 featured DEGs in cell types.

(E) Dot plot showing the GO analysis on the biological process of the top 100 fDEGs.

(F) Dot plot showing the GO analysis on the molecular functions of the top 100 fDEGs.

CPN ligation induced transcriptomic changes in the RSC

The cells from Con (without CPN ligation) and CPN groups were projected in the t-distributed stochastic neighbor embedding (TSNE) based on the transcriptional characteristics (**Figure 5A**), we analyzed the expressional gene difference on these cells. The ECs, Micro, OPC, and Oligo had a higher correlated score between Con and CPN groups based on the genes' mean expressions. In contrast, the *CamkIIα*$^{+}$ neurons, vSMC, and Mac had lower correlation scores (**Figure 5B**), indicating that CPN ligation may induce more significant changes in these cells. We next compared the gene expression difference between the Con and CPN group via the FindMarkers function of Seurat (**Stable 4**). **Figure 5C** presented the differential expressed genes (DEGs) detected on the *CamkIIα*$^{+}$ neurons. Interestingly, those DEGs with larger absolute $\log_{10}$P_Value in *CamkIIα*$^{+}$ neurons also showed altered expressions in other types of cells (**Figure 5D**); this suggests that the expression of some DEGs is impaired in multiple cell types. Further analysis showed that about 18% (124/671, **Stable 5**) upregulated DEGs and 26% (150/572, **Stable 5**) downregulated DEGs were detected at least in two types of cells; the others were differently expressed only on one type of cells (**Figure 5E and F**), indicating that CPN ligation also induced cell-types dependent transcriptomic responses. In line with this, the biological process of (BP) gene ontology (GO) analysis on the upregulated (**Figure 5G, Stable 6**) and downregulated DEGs (**Figure 5H, Stable 7**) showed cell type-dependent functional changes.

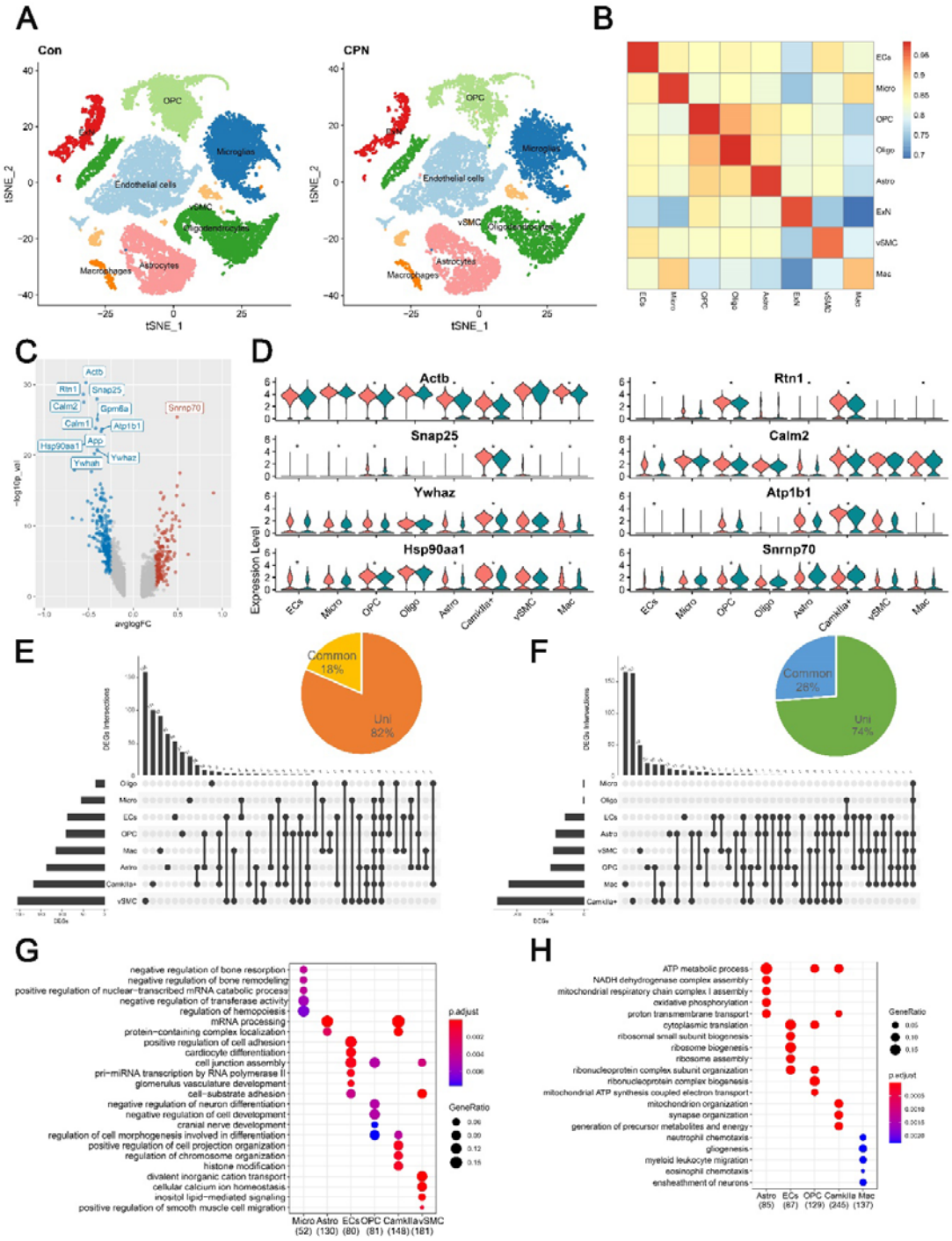

Figure 5. CPN ligation changed the transcriptional profiles of cells in RSC.

(A) *t*-SNE embedding projection of cells from RSC of mice without (Con) or with CPN ligation (CPN).

(B) Heatmap showing the correlations of cell types between two groups.

(C) Volcano plots showing the DEGs between Con and CPN groups detected in *CamkIIα*$^+$ neurons.

(D) Vlnplot to show the expression of the DEGs with larger absolute long10P-Value in the *CamkIIα*$^+$ neurons.

(E) Upset plot showed the distributions of the upregulated DEGs among cell types.

(F) Upset plot showed the distributions of the downregulated DEGs among cell types.

(G) Dot plot showing the GO analysis on the biological process of the upregulated DEGs.

(H) Dot plot showing the GO analysis on the biological process of the downregulated DEGs.

The cell type-dependent functional impairments

The gene-set enrichment analysis (GSEA) indicates the activated or suppressed effects via the positive or negative normalized enriched score (NES), respectively (**Figure 6A**). More important, the GSEA also identified the core enriched genes of the related terms. We performed the GSEA on the DEGs of each type of cell and identified different levels of GO terms. **Figure 6B** presented the ancestor chart of GO term (GO:1902600) proton transmembrane transport; this term is the final child terms of the cellular process and localization of biological process. The directed acyclic graphs showed the relationships of GO terms on biological process (**Figure S2 a-h**) and molecular functions (**Figure S3 a-g**). We detected that this term related to biological functions were suppressed in the Astro, ECs,

CamkIIα^{+} neurons, and Micro. We checked the impaired final child terms on the biological process (**Figure 6C, Stable 8**) and molecular functions (**Figure 6D, Stable 9**) of each cell type. As shown in **Figure 6C and D**, several types of cell have the standard suppressed BP and MF; for example, suppressed mitochondrial related processes were detected in the Astro, ECs, *CamkIIα*$^{+}$ neurons, Oligo, and OPC, and the related molecular functions including the cytochrome-c oxidase activity and the NADH dehydrogenase activities (**Figure 6D**).

Furthermore, nerve injury also induced cell type-dependent BP (**Figure 6E**) and MF changes **(Figure 6F)**. For example, in the Astro, the nucleoside phosphate metabolic process was suppressed. The transcription-related biological process was activated; for the ECs, the epithelium development, tube morphology-related processes were enhanced; these may be involved in the pathological changes of blood vessels under chronic conditions. Unlike this, the oxidative phosphorylation and cell death may be suppressed in the *CamkIIα*$^{+}$ neurons after nerve injury. At the same time, the histone modification was increased, indicating that an epigenetic regulation happens in the *CamkIIα*$^{+}$ neurons. The Mac and Micro also showed differently impaired BPs. For the vSMC, cell migration and cell adhesion-related processes were activated; this may indicate its' functional changes on the regulation of blood vessels. In summary, the peripheral nerve injury-induced cell type-dependent biological processes and molecular functions changes in the RSC.

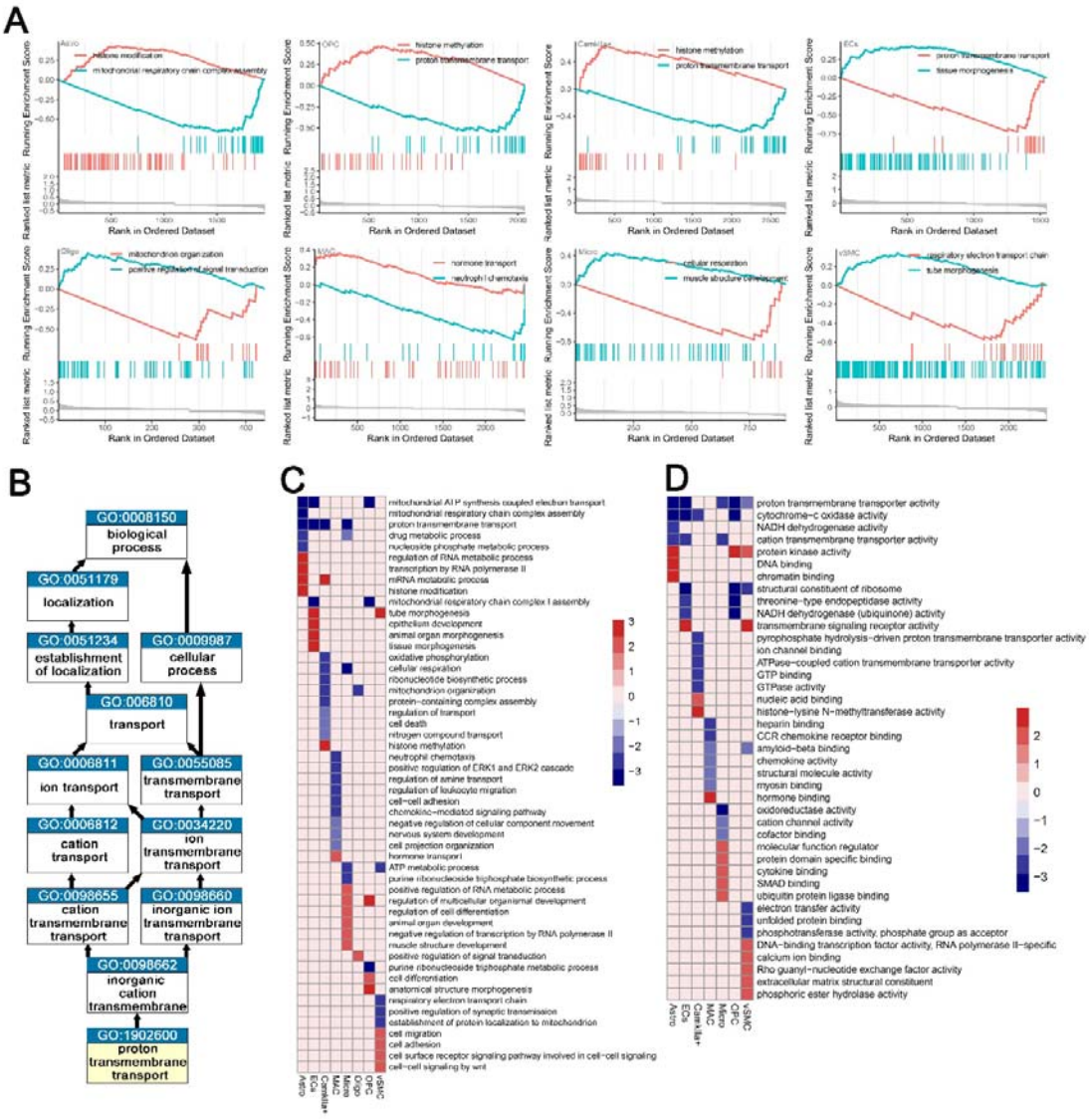

(A) Representative examples showing the activated and suppressed GO terms on BP of each type of cells.

(B) The ancestor chart of GO term (GO:1902600) proton transmembrane transport; this term is the final child term of the cellular process and localization of biological process.

(C) Heatmap showing the NES of the final child terms on the BP analysis. Color indicates the NES of the related term, and positive NES indicates the activated term, and negative NES indicates the suppressed terms.

(D) Heatmap showing the NES of the final child terms on the MF analysis. Color indicates the NES of the related term, and positive NES indicates the activated term, and negative NES indicates the suppressed terms.

The possible changes on the ion channels expressions

The activities of ion channels set up the resting membrane and mediate changes of membrane potentials, therefore, determine neuronal excitability. One possible reason for more c-Fos$^+$ cells in RSC after mechanical stimulation may be the changes in neuronal excitability. We examined the expression of the genes coding the sodium-potassium pump (Na^+/K^+ pump) that determine the resting potentials. As shown in **Figure 7A**, the Na^+/K^+ pump subunits showed a cell type-dependent expressional pattern. The ECs, Micro, and Mac mainly expressed the *Atp1a1* and *Atp1b3*, the OPC, Astro, and vSMC share the same expressional patterns that they mainly expressed *Atp1a2*, and the beta subunits include the *Atp1b1* and *Atp1b2*; while the Na^+/K^+ pump in the Oligo is composed by *Atp1a1* and *Atp1b3*; most of the *CamkIIα*$^+$ cells express *Atp1a3* and *Atp1b1*, some of them also expressed *Atp1a1*.

We detected the downregulated *Atp1a1* in *CamkIIα*$^+$ neurons and decreased *Atp1b1* in Astro and *CamkIIα*$^+$ neurons (**Figure 7B**). At the same time, we observed the decreased *Atp1a2* and *Atp1b1* in *CamkIIα*$^+$ neurons, vSMC, and Mac and higher *Atp1b2* in vSMC. In summary, the CPN ligation changed the expression of the Na^+/K^+ pump units in the Astro, *CamkIIα*$^+$ neurons, vSMC, and Mac. These changes may impair the establishment and maintenance of resting membrane potentials.

The activities of voltage-gated ion channels (VGICs) also affect neuronal excitability. In the RSC, we examined the expression of 88 genes that code VGICs and most of them are enriched in the *CamkIIα*$^{+}$ neurons; some VGICs genes are enriched in other types of cells, such as the *Cacng4* in the OPC and Kcnk1 in Astro (**Figure S4a**). The CPN ligation only increased the expression of two genes (*Cacna2d3*, *Cacna1e*), coding the subunits of voltage-gated calcium channels, but not for sodium and potassium (**Stable 10**). Those observations indicate that the intrinsic properties may not be changed by nerve injury. To confirm this, we performed the whole-cell patch-clamp recording on the splenial neurons (**Figure S4c**); we did not observe any changes on the resting membrane potentials (RMPs) (**Figure S4d**), the half-width (**Figure S4e**), rise and decay time (**Figure S4f and g**) of APs from the CPN group.

The unbalanced Excitatory/Inhibitory synaptic transmission in RSC after nerve injury

The activities of ligand-gated channels convey the information transmitted from other cells and regulate cells' excitability. We examined the expression of ionotropic receptors for the acetylcholine (Ach), Gamma-Aminobutyric Acid (GABA), glycine, glutamate, Inositol 1,4,5-Trisphosphate (ITP), ATP, and Ryanodine (**Figure 7C**). Interestingly, those receptors also showed cell type-dependent expression patterns that the *CamkIIα*$^{+}$ neurons expressed most of the GABA receptors, glutamate receptors subunits as well as the *Itpr1* and *Ryr3*; the Oligo mainly expressed the *Glrb*, *Gria2*, *Gria4*, and *Itpr2*, indicating that the glutamate and glycine are its primary neuronal transmitters. The Mac and Micro expressed the *Gria2*, *P2rx4*, and *P2rx7*, the OPC and Astro also highly expressed *Gria2*, *Grid2*, *Grik5*, *Glrb*, and *Itpr2*, indicating that both types of cells are regulated by the glutamate, glycine, and ITP; moreover, both types of cells expressed different GABARs subunits and NMDARs subunits, for example, the OPC expressed the *Gabrb3* and *Grin3a*, while the Astro expressed the *Gabra2*, *Grbrb1* and *Grin2c*, the OPC also expressed the *Chrna4* which encodes a nicotinic acetylcholine receptor. The vSMC and ECs may respond to glutamate and Itp due to the

expression of *Gria2*, and the ItpRs subunits, respectively. For example, the vSMC expressed *Itpr1* and *Itpr2*, while, the ECs expressed *Itpr2* and *Itpr3*. In summary, the different expressions of the ionotropic receptor subunits indicate the variety of the major regulation factors for these cells.

We next examine the effects of nerve injury on the expression of ligand-gated ion channels (LGICs). In our system, CPN ligation may change the cellular responses to the GABA, glycine, glutamate, ITP, and Ryanodine in the RSC (**Figure 7D**). We detected a higher level of *Gria1* and *Ryr2* in *CamkIIα*$^+$ neurons, and also the increased *Gria2* in OPC, Oligo, and Astro, upregulated *Grin2c* in Astro; these results indicate that the glutamate mediating synaptic regulations may be enhanced in the *CamkIIα*$^+$ neurons, OPC, Oligo and Astro; in contrast, we detected lower levels of *Gabra1* and *Glrb* in *CamkIIα*$^+$ neurons. These may indicate that the decreased inhibitory synaptic transmissions in the RSC. To confirm this point, we performed the whole-cell patch-clamp recording in the RSC neurons. In addition, we recorded the spontaneous excitatory postsynaptic currents (sEPSCs) and inhibitory postsynaptic currents (sIPSCs) by holding the membrane potential at -70 mV or 10 mV, respectively; and the application of CNQX or picrotoxin significantly blocked these currents (**Figure 7E**), indicating that these currents were AMPARs or GABARs mediated. In line with the transcriptional changes, we observed a higher amplitude of sEPSCs and a lower frequency and amplitude of IPSCs on the *CamkIIα*$^+$ neurons (**Figure 7F and G**). Therefore, the CPN ligation did change the E/I synaptic balance in the RSC. These data indicate that the processing of the input information in the RSC was increased, this may lead to the over excitability of RSC neurons after nerve injury.

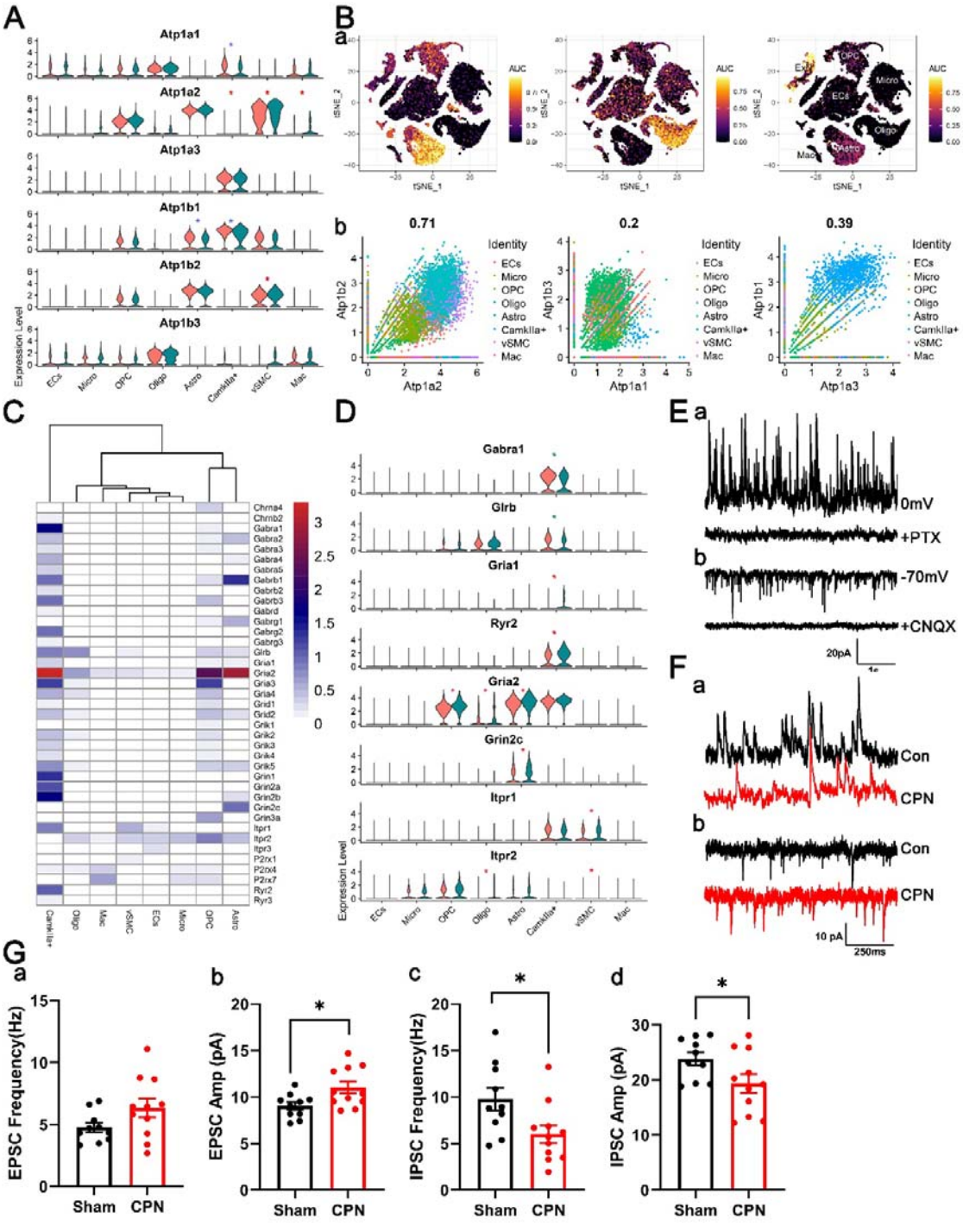
A
Atp1a1
Atp1a2
Atp1a3
Atp1b1
Atp1b2
Atp1b3
Expression Level
ECs
Micro
OPC
Oligo
Astro
CamKIIa+
vSMC
Mac
B
a
AUC
tSNE_1
tSNE_2
b
0.71
0.2
0.39
Identity
Atp1b2
Atp1a2
Atp1b3
Atp1a1
Atp1b1
Atp1a3
C
D
Gabra1
Glrb
Gria1
Ryr2
Gria2
Grin2c
Itpr1
Itpr2
E
a
0mV
+PTX
b
-70mV
+CNQX
20pA
F
a
Con
CPN
b
10 pA
250ms
G
a
EPSC Frequency(Hz)
b
EPSC Amp (pA)
c
IPSC Frequency(Hz)
d
IPSC Amp (pA)
Sham
CPN

Figure 7. CPN ligation changed the excitatory/inhibitory synaptic transmission balance in the RSC.

(A) The vlnplot showing the expression of Na^+/K^+ pump subunits in the RSC. * in red indicates upregulation, * in blue indicates downregulation.

(B) The cell types dependent expression of Na^+/K^+ pump subunits. a, TSNE plot shows the expression of *Atp1a2*, *Atp1b1* and *Atp1b2* (left), the *Atp1a1* & *Atp1b3* (middle), and the *Atp1a3* & *Atp1b1* (right) in different types of cells. b, the feature scatter plot showing the co-expression of the Na^+/K^+ pump subunits, *Atp1a2* & *Atp1b2* (left), *Atp1a1* & *Atp1b3* (middle), *Atp1a3* & *Atp1b1* (right).

(C) Heatmap showing the cell-types dependent expression of the ligand-gated ion channels subunits in the RSC.

(D) Vlnplot showing the different expression of Grbra1, Glrb, Gria1, Gria2, Ryr2, Grin2c, Itpr1, Itpr2 in the Con and CPN condition. * in red indicates upregulation, * in blue indicates downregulation.

(E) a, Presented examples showed that the spontaneous currents recorded at 0 mV (upper) were blocked by picrotoxin (lower). b, the presented examples showing the recorded AMPARs mediating sEPSCs, these currents recorded at -70 mV (upper) were blocked by CNQX (lower).

(F) the presented examples show the recording of sIPSCs (a) and sEPSCs (b) at Con and CPN conditions.

(G) Summarized data showed that the amplitude of sEPSCs were enhanced, while the frequency and amplitude of sIPSCs were decreased in CPN.

CPN ligation impaired the cell-cell communications in the RSC

The Cell-cell communications via the cytokine and growth factors are critical for the functions of brain regions. We next examined the cell talk patterns via the cytokine and growth factors in the RSC (**Figure 8A and B**). As shown in **Figure 8Aa**, the cells in RSC communicate broadly via the cytokine. For example, the ECs secreted *Cxcl12* and communications with Mac, Micro, Oligo, OPC, and vSMC via different receptors, such as the *Itgb1*, *Sdc4*, *Ackr3*, *Cxcr3*, *Cd4*, and *Cxcr4*. The *CamkIIα*$^+$ neurons released *Cx3cl1* to affect the Mac and Micro via its receptor *Cx3cr1*; at the same time, the vSMC generated *Il34*, which would bind to the *Csf1r* on Micro and Mac (**Figure 8Ab**). The growth factors also contribute to the cells' talk in RSC (**Figure 8Ba**). The ECs highly expressed the *Flt1*, which bound the *Vegfa* released from Oligo, OPC, Astro, and *Vegfb* secreted from Mac, Micro, Oligo, OPC, Astro. At the same time, the ECs secreted *Hbegf* and *Pdgfb*, which regulated Oligo and OPC, respectively. The expression of *Cd9* on the Oligo allowed it to receive the *Hbegf* from ECs, Astro, vSMC, and OPC (**Figure 8Bb**). In summary, there are different types of cell talks in the RSC mediating by different cytokines and growth factors.

The CPN ligation changed the cytokine mediating cell talk (**Figure 8Ac**). As shown in **Figure 8Ac** and **C**, higher *Ccl2* and *Il16* were detected in the Micro following with the increased expression of their receptors in the target cells. While the level of *Ccl12* in Mac and *Cx3cl1* in *CamkIIα*$^+$ neurons decreased, in contrast, their receptors, *Ccr5* and *Cx3cr1* in Micro increased. Furthermore, the CPN ligation also changed the expression of growth factors and their receptors (**Figure 8Bc**), and the impaired cell talks mainly happened among the Micro, OPC, Oligo, Astro, vSMC, and ECs (**Figure 8D**).

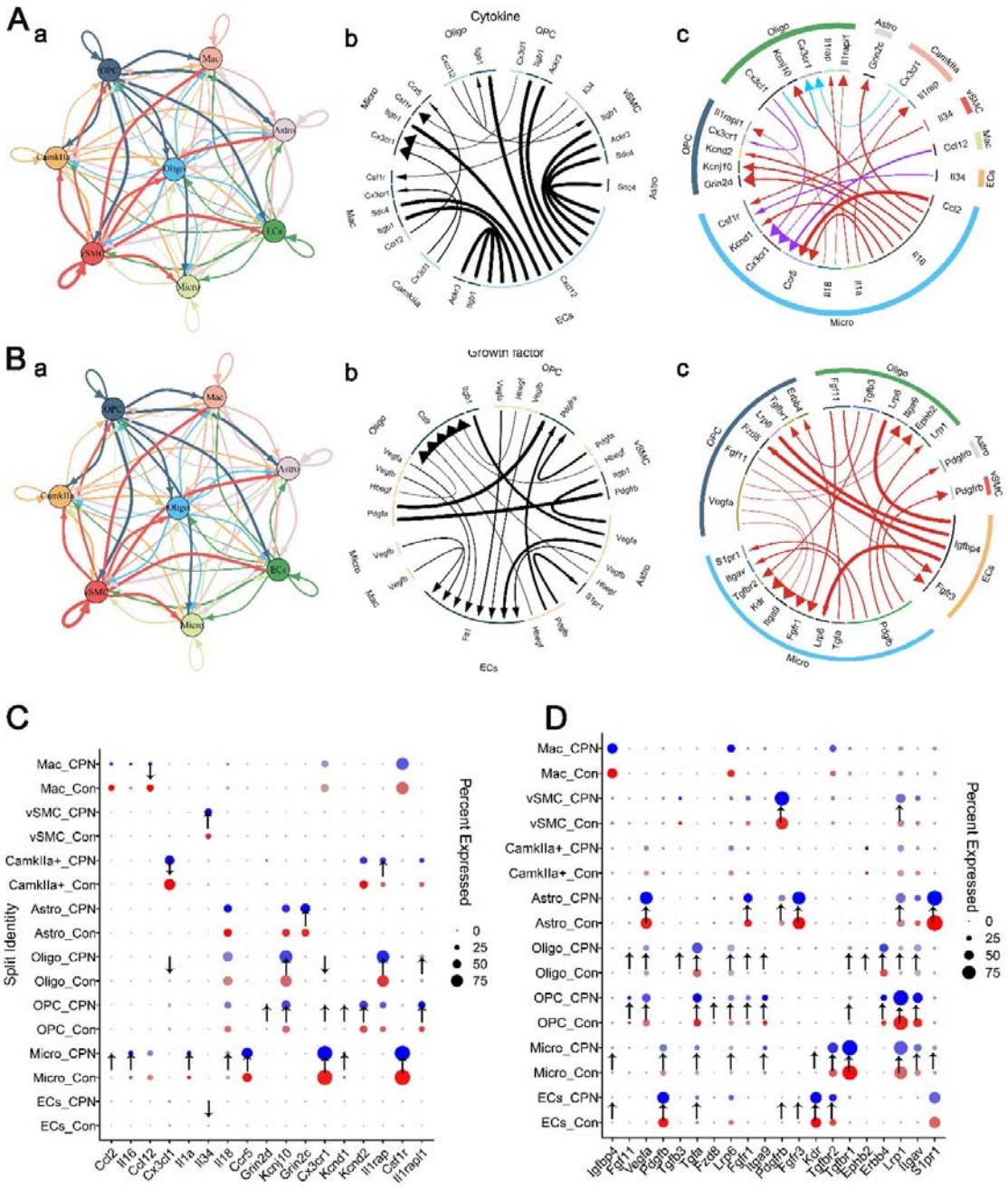

Figure 8. CPN ligation impaired the cell-cell communications via the cytokine and growth factors.

(A) The cytokine mediates cell talks in the RSC. a, the network plot showing the basic cytokine mediating cell talks in the RSC. b, Circle plot showing the top 20 ligand-receptors

pairs of cytokine communications. c, Circle plot showing the top 20 pairs of changed ligand-receptors in the RSC.

(B) The growth factor mediates cell talks in the RSC. a, the network plot showing the growth factors mediating cell talks in the RSC. b, Circle plot showing the top 20 ligand-receptors pairs of growth factor communications. c, Circle plot showing the top 20 pairs of changed ligand-receptors of growth factor in the RSC.

(C)Dot plot showing the detailed changes of the ligand-receptors pairs in Ac.

(D) Dot plot showing the detailed changes of the ligand-receptors pairs in Bc.

Discussion

In the current study, we investigated the transcriptomic changes in the RSC after peripheral nerve injury. Our data showed that selectively activating CamKIIα$^+$ neurons in RSC decreased PWTs and induced conditioned place aversion in naïve mice. Reversely, inactivating the CamKIIα$^+$ neurons increased the PWTs of mice with nerve injury. Furthermore, using a single-cell RNA sequencing approach we found that in the mice with CPN ligation, cell type-dependent transcriptomic changes affected the mitochondrial functions, cell-cell communications, and excitatory/inhibitory synaptic transmissions. Our study, therefore, provided a piece of novel information about the cell type-dependent changes on the transcriptomic level; our data indicate that the RSC is a critical brain region for the pain regulation, and knowing the transcriptional changes in RSC would help to understand the molecular mechanism for the maintenance of neuropathic pain.

The E/I synaptic unbalance in the RSC impaired the pain sensation

The E/I synaptic balance is critical for the brain functions [35]. After nerve injury, the E/I unbalance generally happed along the somatosensory pathway that contribute to the persistent of chronic pain [36–38]. Here we showed that E/I unbalance in the RSC after nerve injury. We

examined the expressions of ligand-gated ion channels (LGICs) to the primary neuronal transmitters, such as the glutamate, glycine, GABA, and ACH in the RSC. Our results showed the cell type-dependent expression patterns of the LGICs, such as the *Gria2*, which mainly expressed in the *CamkIIα*$^+$ neurons, OPC, and Astro. In contrast, the *Chnra4*, which codes the nicotinic alpha 4 subunits of the cholinergic receptor, is dominantly expressed in the OPC, indicating its unique role in regulating OPC's function. Furthermore, we observed the increased *Gria1*, which codes a subunit of AMPARs, the primary inotropic glutamate receptors, and decreased *Gabra1* and *Glrb* in the *CamkIIα*$^+$ neurons; these results indicate that the E/I unbalance after CPN ligation. In line with this, our electrophysiological recording results confirmed this and showed higher amplitudes of sEPSCs but lower amplitude and frequency of sIPSCs in the RSC. This result provides information about the E/I synaptic unbalance in the RSC. It also indicates the usefulness of transcriptional information in understanding the molecular mechanisms of neuropathic pain.

We also examined the cell-types dependent expressions of subunits of Na^+/K^+ pump in the RSC, our results indicate a different expressional patter of *CamkIIα*$^+$neurons to other cell types. More important, we observed the decreased expression of *Atp1a2* and *Atp1b1* in *CamkIIα*$^+$ neurons. While our whole-cell patch-clamp recording results did not show this change on RMP, the mismatch indicates that the transcriptional changes may induce the protein changes later. In analyzing the expressions of VGICs, we detected the different changes on *Cacna2d3* and *Cacna1e*, which may pass through more Ca^{2+} during the bursting of action potentials. In summary, our scRNA-seq data not only indicates the possible E/I unbalance in the RSC, it also provides the information about the cell-types dependent expressions of VGICs and LGICs, which would help to understand the basic physiology of different cell types in the RSC.

Cell-cell communications are critical for the functions of specific brain functions. By taking the advantages of scRNA-seq, we examined the communication patterns of the growth factors, cytokines, and their receptors. Our scRNA-seq data strongly indicate that the cell talk patterns are cell type-dependent in the RSC. The CPN ligation changes both growth factors and cytokine-mediated cells' talk, indicated by the increased growth factors and their receptors on the Oligo and OPC. However, among the top 20 pairs of ligand-receptors on the cytokine and growth factors, there are not any noticeable expression changes observed in the *CamkIIα*$^{+}$ neurons, these observations indicate the major cell talks patterns among other cell types are different from the *CamkIIα*$^{+}$ neurons. Based on our scRNA-seq results, we proposed that the thalamic neurons may send the noxious information first to the *CamkIIα*$^{+}$ neurons (**Figure 9**), these neurons also send the related information to other types of cells via the glutamate mediating synaptic transmissions. After nerve injury, the enhanced noxious information may activate more *CamkIIα*$^{+}$ neurons, and further induce the pathological cell talks among other cell types via the released cytokine and growth factors. Therefore, lead to peripheral pain sensitization. The contributions of the changed cytokine and growth factors to peripheral pain sensitivity need to be further studied.

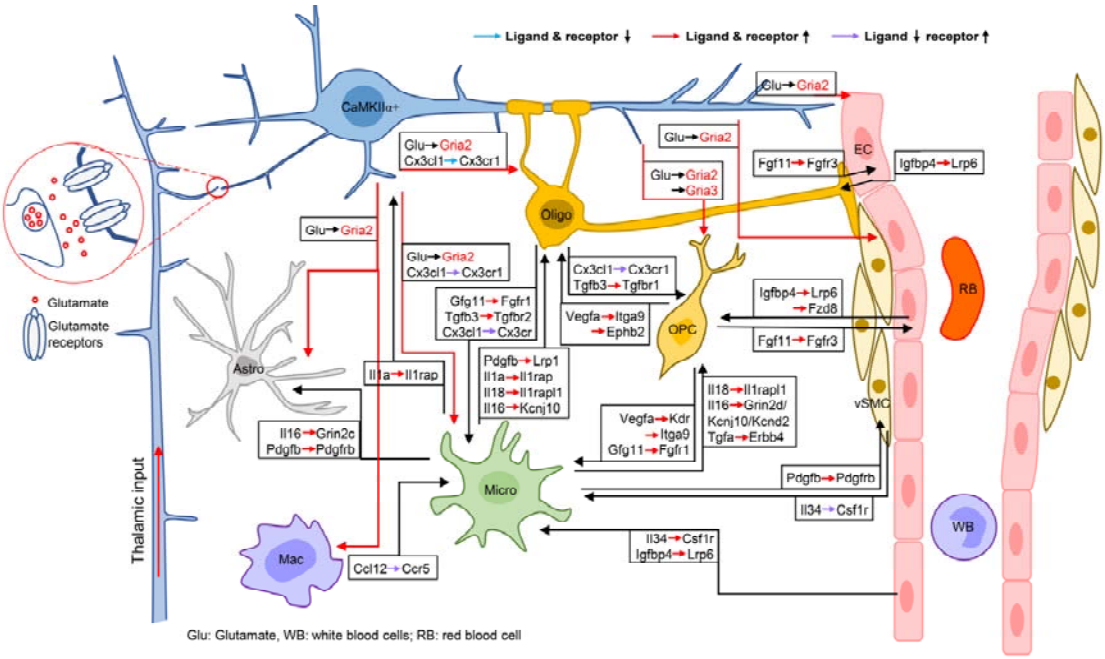

Figure 9. A carton presents the major changed Cell-Cell communications in the RSC after nerve injury.

Understanding the cellular mechanisms of neuropathic pain based on scRNA-seq results

Here we provide the transcriptomic profiles of the RSC cells, we identified the featured DEGs of each cell type, we also examined the cell talks patterns, including growth factors, cytokine and the major neuronal transmitters and observed the cell-types specific communications in the RSC, these data would help to understand the coordination among the splenial cells.

Our data also indicate that the CPN ligation induced broadly transcriptional changes in the RSC, and most of the DEGs were cell type-dependent. For example, over 70% of the DEGs were unique to the related cell types. Moreover, the GO analysis on these DEGs also showed the cell type-dependent changes on the biological process and molecular functions; further, GSEA results also confirm this point. Considering the unique roles of different cell types in the CNS, the cell-types dependent changes may contribute to the pathological

changes in the brain and lead to peripheral pain hypersensitivity and comorbid anxiety or depressive symptoms. These data thus emphasized the cell-types dependent molecular changes in the RSC after nerve injury. And the role of genes changes in specific cell types should be further studied.

The neurons in RSC regulates peripheral pain sensation

In the current study, our data manifested that enhancing the activities of *CamKIIα*$^+$ neurons decreased the PWTs of naïve mice and also shortened the thermal withdrawal latency. RSC's regulation on pain sensation lasts for less than 24 hours; this implies that the regulation is not persistent. Given that the noxious information was presented in the RSC, evaluated by both electrophysiological recording [13] and brain imaging [39], these noxious responses may further facilitate the peripheral pain sensation via the descending regulation. Enhancing the activities of *CamKIIα*$^+$ neurons in RSC also induced place aversion. A previous study showed that the formalin injection induced aversion with c-Fos expression in the RSC [20]. Here we clearly showed that enhancing the glutamatergic neuronal activities is sufficient to induce aversion. Given that the RSC is tightly connected with the hippocampal formation [40,41] and is involved in spatial cognition [41–45], the place aversion may come from the integration of the spatial information [15,17]. Previous studies showed that the primary somatosensory cortex (S1), the anterior cingulate cortex (ACC) [46], central amygdala [47], nucleus accumbens [48], and parabrachial nucleus [49] form a neuronal network for the regulation of pain aversion [50]. Our observation suggests that the RSC is one of the brain regions for the code of aversion.

Our results are different from the previous studies that RSC's electrical stimulation has analgesic effects on tail-flick and formalin-induced pain [51–54]. Different stimulating methods may activate various neuronal assemblies in RSC. As we all know, electrical stimulations would trigger all types of cells in RSC, including glutamatergic and GABAergic neurons. While the chemogenetic approach selectively activated the *CamKIIα*$^+$ neurons in RSC in the

current study, this may lead to the different effects on the regulation of RSC to pain sensation. In summary, we provide a piece of evidence that the activities of *CamKIIα*$^{+}$ neurons in RSC facilitate peripheral pain sensation.

Acknowledgments:

We thank Dr. San-Hua Fang at Core Facilities of the School of Medicine, Zhejiang University. The authors apologize to colleagues whose work could not be cited due to space and reference restrictions.

Author contributions: JH Wang performed western blots, immunostaining, mechanical allodynia testing, and data analysis. YN Lian performed patch-clamp recording experiments. L Liu carried out the immunostaining experiments and data analysis. W Chen and W Chen performed the virus injection and data analysis. Z Zhang and M Zhuo designed experiments performed data analysis and approved the draft. XY Li designed experiments, performed data analysis, and wrote the paper.

Conflict of interest: The authors declare that they have no known competing financial interests or personal relationships that could have appeared to influence the work reported in this paper.

Funding:

This study was supported by the National Natural Science Foundation of China (81571068, 31871062, 81801102, and 31771157), Youth Program of National Natural Science Foundation of China (No. 81801279), the Fundamental Research Funds for the Central Universities, the MOE Frontier Science Center for Brain Science & Brain-Machine Integration, Zhejiang University.

References

[1] J. Dahlhamer, J. Lucas, C. Zelaya, R. Nahin, S. Mackey, L. DeBar, R. Kerns, M. Von Korff, L. Porter, C. Helmick, *MMWR. Morb. Mortal. Wkly. Rep.* **2018**, *67*, 1001.

[2] L. Colloca, T. Ludman, D. Bouhassira, R. Baron, A. H. Dickenson, D. Yarnitsky, R. Freeman, A. Truini, N. Attal, N. B. Finnerup, C. Eccleston, E. Kalso, D. L. Bennett, R. H. Dworkin, S. N. Raja, *Nat. Rev. Dis. Prim.* **2017**, *3*, DOI 10.1038/nrdp.2017.2.

[3] M. Costigan, J. Scholz, C. J. Woolf, *Annu. Rev. Neurosci.* **2009**, *32*, 1.

[4] M. Calvo, A. J. Davies, H. L. Hébert, G. A. Weir, E. J. Chesler, N. B. Finnerup, R. C. Levitt, B. H. Smith, G. G. Neely, M. Costigan, D. L. Bennett, *Neuron* **2019**, *104*, 637.

[5] S. Tang, H. Jing, Z. Huang, T. Huang, S. Lin, M. Liao, J. Zhou, *J. Cell. Biochem.* **2020**, *121*, 1635.

[6] R. Kuner, T. Kuner, *Physiol. Rev.* **2021**, *101*, 213.

[7] R. R. Ji, C. R. Donnelly, M. Nedergaard, *Nat. Rev. Neurosci.* **2019**, *20*, 667.

[8] M. Tsuda, *Neurosci. Bull.* **2018**, *34*, 178.

[9] C.-L. Li, K.-C. Li, D. Wu, Y. Chen, H. Luo, J.-R. Zhao, S.-S. Wang, M.-M. Sun, Y.-J. Lu, Y.-Q. Zhong, X.-Y. Hu, R. Hou, B.-B. Zhou, L. Bao, H.-S. Xiao, X. Zhang, *Cell Res.* **2016**, *26*, 83.

[10] G. Hu, K. Huang, Y. Hu, G. Du, Z. Xue, X. Zhu, G. Fan, *Sci. Rep.* **2016**, *6*, 1.

[11] J. K. Niehaus, B. Taylor-Blake, L. Loo, J. M. Simon, M. J. Zylka, *Neuron* **2021**, *109*, 1274.

[12] J.-A. Yang, J.-M. He, J.-M. Lu, L.-J. Jie, *J. Cell. Biochem.* **2018**, *119*, 4792.

[13] R. W. Sikes, L. J. Vogt, B. A. Vogt, *Pain* **2008**, *135*, 160.

[14] G. C. Quintero, *J. Pain Res.* **2013**, *6*, 713.

[15] G. Vantomme, Z. Rovó, R. Cardis, E. Béard, G. Katsioudi, A. Guadagno, V. Perrenoud, L. M. J. Fernandez, A. Lüthi, *Cell Rep.* **2020**, *31*, DOI 10.1016/j.celrep.2020.107747.

[16] J. P. Shine, J. P. Valdés-Herrera, M. Hegarty, T. Wolbers, *J. Neurosci.* **2016**, *36*, 6371.

[17] A. S. Alexander, D. A. Nitz, *Curr. Biol.* **2017**, *27*, 1551.

[18] J. T. Da Silva, D. A. Seminowicz, *Pain reports* **2019**, *4*, e732.

[19] P. E. Paulson, T. J. Morrow, K. L. Casey, *Pain* **2000**, *84*, 233.

[20] L. G. Lei, Y. Q. Zhang, Z. Q. Zhao, *Neuroreport* **2004**, *15*, 67.

[21] C. E. Kim, Y. K. Kim, G. Chung, H. J. Im, D. S. Lee, J. Kim, S. J. Kim, *Neuroimage* **2014**, *86*, 311.

[22] C. S. Chiou, C. C. Chen, T. C. Tsai, C. C. Huang, D. Chou, K. Sen Hsu, *Anesthesiology* **2016**, *125*, 779.

[23] K. I. Vadakkan, Y. H. Jia, M. Zhuo, *J. Pain* **2005**, *6*, 747.

[24] S. R. Chaplan, F. W. Bach, J. W. Pogrel, J. M. Chung, T. L. Yaksh, *J. Neurosci. Methods* **1994**, *53*, 55.

[25] Y. J. Wang, Z. X. Zuo, C. Wu, L. Liu, Z. H. Feng, X. Y. Li, *Front. Mol. Neurosci.* **2017**, DOI 10.3389/fnmol.2017.00289.

[26] M. Leger, A. Quiedeville, V. Bouet, B. Haelewyn, M. Boulouard, P. Schumann-Bard, T. Freret, *Nat. Protoc.* **2013**, *8*, 2531.

[27] G. J. Brewer, J. R. Torricelli, *Nat. Protoc.* **2007**, *2*, 1490.

[28] S. Zhong, W. Ding, L. Sun, Y. Lu, H. Dong, X. Fan, Z. Liu, R. Chen, S. Zhang, Q. Ma, F. Tang, Q. Wu, X. Wang, *Nature* **2020**, *577*, 531.

[29] T. Stuart, A. Butler, P. Hoffman, C. Hafemeister, E. Papalexi, W. M. 3rd Mauck, Y. Hao, M. Stoeckius, P. Smibert, R. Satija, *Cell* **2019**, *177*, 1888.

[30] G. Yu, L. G. Wang, Y. Han, Q. Y. He, *Omi. A J. Integr. Biol.* **2012**, *16*, 284.

[31] Y. Wang, R. Wang, S. Zhang, S. Song, C. Jiang, G. Han, M. Wang, J. Ajani, A. Futreal, L. Wang, *bioRxiv* **2019**, 507871.

[32] C. Katche, J. H. Medina, *Cereb. Cortex* **2017**, *27*, 1060.

[33] D. A. Barrière, A. M. Hamieh, R. Magalhães, A. Traoré, J. Barbier, J. M. Bonny, D. Ardid, J. Busserolles, S. Mériaux, F. Marchand, *Pain* **2019**, *160*, 2241.

[34] T. V. P. Bliss, G. L. Collingridge, B. K. Kaang, M. Zhuo, *Nat. Rev. Neurosci.* **2016**, *17*, 485.

[35] N. Z. Gungor, J. Johansen, *Neuron* **2019**, *102*, 903.

[36] F. Le Cao, M. Xu, K. Gong, Y. Wang, R. Wang, X. Chen, J. Chen, *J. Pain* **2019**, *20*, 917.

[37] D. Vecchia, D. Pietrobon, *Trends Neurosci.* **2012**, *35*, 507.

[38] M. Petrou, R. Pop-Busui, B. R. Foerster, R. A. Edden, B. C. Callaghan, S. E. Harte, R. E. Harris, D. J. Clauw, E. L. Feldman, *Acad. Radiol.* **2012**, *19*, 607.

[39] G. Wik, H. Fischer, B. Bragée, M. Kristianson, M. Fredrikson, *Neuroreport* **2003**, *14*, 619.

[40] J. Sugar, M. P. Witter, N. M. van Strien, N. L. M. Cappaert, *Front. Neuroinform.* **2011**, *5*, DOI 10.3389/fninf.2011.00007.

[41] N. Yamawaki, K. A. Corcoran, A. L. Guedea, G. M. G. Shepherd, J. Radulovic, *Cereb. Cortex* **2019**, *29*, 2728.

[42] A. N. Opalka, D. V. Wang, *Learn. Mem.* **2020**, *27*, 310.

[43] S. D. Vann, J. P. Aggleton, E. A. Maguire, *Nat. Rev. Neurosci.* **2009**, *10*, 792.

[44] A. M. P. Miller, L. C. Vedder, L. M. Law, D. M. Smith, *Front. Hum. Neurosci.* **2014**, *8*, 586.

[45] A. S. Mitchell, R. Czajkowski, N. Zhang, K. Jeffery, A. J. D. Nelson, *Brain Neurosci. Adv.* **2018**, *2*, 239821281875709.

[46] X. B. Wu, L. N. He, B. C. Jiang, X. Wang, Y. Lu, Y. J. Gao, *Neurosci. Bull.* **2019**, *35*, 613.

[47] G. Corder, B. Ahanonu, B. F. Grewe, D. Wang, M. J. Schnitzer, G. Scherrer, *Science (80-.).* **2019**, *363*, 276.

[48] R. Al-Hasani, J. G. McCall, G. Shin, A. M. Gomez, G. P. Schmitz, J. M. Bernardi, C. O. Pyo, S. Il Park, C. M. Marcinkiewcz, N. A. Crowley, M. J. Krashes, B. B. Lowell, T. L. Kash, J. A. Rogers, M. R. Bruchas, *Neuron* **2015**, *87*, 1063.

[49] M. C. Chiang, A. Bowen, L. A. Schier, D. Tupone, O. Uddin, M. M. Heinricher, *J. Neurosci.* **2019**, *39*, 8225.

[50] R. Du, W. J. Luo, K. W. Geng, C. L. Li, Y. Yu, N. Wei, J. Chen, *Neurosci. Bull.* **2020**, *36*, 649.

[51] G. M. Reis, R. S. Fais, W. A. Prado, *Pharmacol. Biochem. Behav.* **2015**, *131*, 112.

[52] G. M. Reis, A. C. Rossaneis, J. W. S. Silveira, Q. M. Dias, W. A. Prado, *J. Pain* **2011**, *12*, 523.

[53] G. M. Reis, Q. M. Dias, J. W. S. Silveira, F. Del Vecchio, N. Garcia-Cairasco, W. A. Prado, *J. Pain* **2010**, *11*, 1015.

[54] A. C. Rossaneis, G. M. Reis, W. A. Prado, *Pharmacol. Biochem. Behav.* **2011**, *100*, 220.